International Symposium
On Turbulence and Shear Flow
Phenomena (TSFP-9)
June 30 - July 3, 2015 *Melbourne, Australia*

NUMERICAL DISSIPATION AND SGS MODELING IN LES OF LAMINAR SEPARATION BUBBLE FLOWS

F. Cadieux, J. A. Domaradzki
Department of Aerospace and Mechanical Engineering
University of Southern California
Los Angeles, CA 90089-1191
cadieux@usc.edu

ABSTRACT

Laminar separation bubbles develop over many blades and airfoils at moderate angles of attack and Reynolds numbers ranging from 10^4 to 10^5. More accurate simulation tools are necessary to enable higher fidelity design optimization for these airfoils and blades as well as to test flow control schemes. An equivalent problem is formulated by imposing suitable boundary conditions for flow over a flat plate to avoid numerical and mesh generation issues. LES of such a flow were performed at drastically reduced resolution using a spectral solver to unambiguously assess the accuracy of LES in which filtering is used to replace explicit subgrid-scale (SGS) modeling – a filter (F1), a weaker filter (F2), and the truncated Navier-Stokes with automatic filtering (TNS) – and compare it to the dynamic Smagorinsky model. The performance of each LES is evaluated against benchmark DNS data focusing on pressure and skin friction distributions, which are critical to airfoil designers. TNS and F2 results confirm that filtering can act as an apt substitute for explicit SGS models, whereas the poor predictions of F1 circumscribe the possible dangers of grid and filter-width dependence of this approach.

INTRODUCTION

The flow over many blades and airfoils at moderate angles of attack and Reynolds numbers ranging from 10^4 to 10^5 undergoes separation-induced transition due to the adverse pressure gradient generated by surface curvature, forming a laminar separation bubble. This phenomenon can favorably increase lift-over-drag ratio on the wings of small unmanned aircraft by promoting early transition to turbulence and flow reattachment. In turbine flows, it causes unsteady structural loading which can lead to fatigue and reduce blade lifecycle. Ways to control or delay the onset of separation, transition and reattachment for these applications are sought at the design stage.

An equivalent problem is formulated by imposing suitable boundary conditions for flow over a flat plate to avoid numerical and mesh generation issues. Spalart & Strelets (2000) tested a number of Reynolds-averaged Navier-Stokes (RANS) turbulence models for such a laminar separation bubble flow. Spalart-Allmaras results recovered the peak negative skin friction value and location, but over-predicted the reattachment point. Other turbulence models transitioned and reattached early. Peak negative skin friction predicitons varied widely from one model to the next, and no model recovered the turbulent skin friction downstream of reattachment of the DNS. Howard *et al.* (2000), Hadžić & Hanjalić (2000), and Papanicolaou & Rodi (1999) tested other RANS turbulence models with modifications to improve transition prediction for similar problems. The models predicted the location of transition and reattachment more reliably, but their predictions for the peak negative skin friction and skin friction levels downstream of reattachment differed significantly from model to model and generally did not recover DNS values.

More accurate simulation tools are necessary to enable higher fidelity design optimization of airfoils and blades operating at moderate Reynolds numbers as well as to test flow control schemes. Cadieux *et al.* (2014) and Castiglioni *et al.* (2014) recently demonstrated that fast and accurate LES of laminar separation bubble flows are attainable with as low as 1% of DNS resolution. The focus of this work is to investigate whether the proposition made by Rizzetta *et al.* (2003), Bogey & Bailly (2006), Minguez *et al.* (2008), and Tantikul & Domaradzki (2010) that explicit filtering or damping affecting only the smallest resolved scales can act as an effective subgrid-scale (SGS) model holds for highly under-resolved simulations of a laminar separation bubble flow over a flat plate. The performance of different explicitly-filtered simulations and LES with the dynamic Smagorinsky model is compared to DNS benchmark data provided by Spalart & Strelets (2000). Focus is placed on accurately predicting time-averaged pressure (C_p) and skin friction (C_f), which are of critical importance to airfoil and blade designers. Mean and RMS velocity profiles are also considered.

METHOD

The computational setup of Spalart & Strelets (2000) to simulate a laminar separation bubble flow over a flat plate using suction from the top is used and described in figure 1. The Reynolds number at the location of the peak suction velocity is $Re_x = 10^5$. The vertical suction velocity is specified as

$$V(x) = a\exp(-[(x-x_s)/(0.24Y)]^2), \qquad (1)$$

where a is the peak velocity and x_s is its streamwise location. The resulting separation bubble is sensitive only to the upper-wall boundary conditions through the nominal flow deceleration parameter $S = \frac{1}{YU_0}\int V(x)dx$. Using the height

Y to non-dimensionalize all relevant lengths henceforth, the parameters in the equations above are set such that $x_s = 3$, $S = 0.3$ and the Reynolds number at x_s is $Re_{x_s} = 10^5$, giving $a \approx 0.7U_0$ and $Re_Y = Re_{x_s}/3$. These choices are driven by the requirement that the flow separates naturally, without additional forcing mechanisms that were otherwise necessary in the DNS by Alam & Sandham (2000). This setup also ensures a favorable comparison with pressure distributions and the Reynolds number based on bubble length ($Re = 6.7 \times 10^4$) of laminar separation bubble flows seen on the suction side of airfoils.

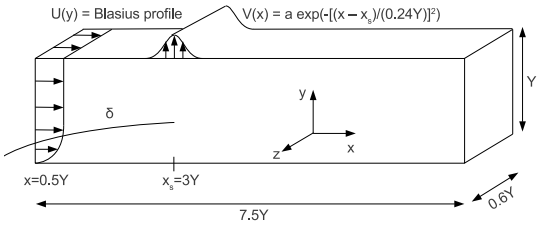

Figure 1: Physical domain, boundary and inlet conditions used to investigate laminar separation bubble flow.

Kravchenko & Moin (1997) showed that numerical dissipation due to derivative and flux approximations in highly under-resolved simulations can become of the same order of magnitude as the SGS dissipation provided by explicit models. Stabilizing filters can also have a similar impact on results and adding an explicit SGS model may deteriorate results as demonstrated in Cadieux *et al.* (2014). A Fourier-Chebyshev pseudo-spectral solver with no stabilizing filter is thus chosen to unambiguously evaluate the performance of different filtering approaches and SGS models without numerical dissipation. The incompressible LES equations are integrated in time using a classic pressure-correction method outlined in Guermond *et al.* (2006). Boundary conditions that lead to $O(\Delta t^3)$ accuracy are chosen based on the Zang-Hussaini algorithm described in Canuto *et al.* (2007). Algebraic mapping is used to cluster points inside the boundary layer and away from the top wall. Sponge regions spanning $x = 0.25$ to $x = 0.45$ and $x = 8.7$ to $x = 10$ are used to recycle the outflow back to the desired Blasius inflow profile. The physically representative region of the computational domain spans $x = 0.5$ to $x = 7.5$. Suction from the top and blowing at the wall induces a 25% deceleration in the mean flow and ensure that mass is conserved through the global pressure-correction step. Blowing through the wall severely limits the CFL restriction, increasing our computational time from a few hours to one day. It also removes any possibility of implicit filtering in time due to large time steps.

If the small scales of turbulence are responsible for kinetic energy dissipation, filtering the smallest resolved scales at each time step can act as an effective way to introduce such dissipation where it might otherwise be negligible – as it is when using high-order solvers. The underlying problem of using filtering to replace a SGS model then becomes defining a filter operation and its length scale such that it provides the correct amount of dissipation for different grids and different flows in the same way that explicit SGS models like the dynamic Smagorinsky are deemed universal. Despite this difficulty, explicitly-filtered LES with no models, also called implicit LES (or ILES), have had success in a number of applications detailed in Rizzetta *et al.* (2003) and Bogey & Bailly (2006), and more recently laminar separation bubble flows as demonstrated in Cadieux *et al.* (2014). To investigate this alternative approach to LES, two low-pass filters F1 and F2 consisting of the product of an approximate deconvolution filter $Q_N \approx G^{-1}$ with filter kernel G as described in Stolz *et al.* (2001) and Tantikul & Domaradzki (2010) are implemented in physical space and used at every time step as a replacement for a SGS model:

$$Q_N G = I - (I - G)^{N+1}. \tag{2}$$

$N = 5$ is chosen such that both filters only attenuate scales smaller than $\Delta = 2\Delta x$. Filter F1 is defined as $Q_5 G_1(\Delta x)$ where the kernel G_1 is a simple three point filter:

$$G_1(\Delta x) * f(x) \approx \frac{1}{8} f(x-\Delta x) + \frac{3}{4} f(x) + \frac{1}{8} f(x+\Delta x). \tag{3}$$

The second, weaker filter F2 is defined similarly as $Q_5 G_2(\Delta x)$ where the kernel G_2 is designed to remove less energy from the small resolved scales:

$$G_2(\Delta x) * f \approx \frac{1}{12} f(x-\Delta x) + \frac{5}{6} f(x) + \frac{1}{12} f(x+\Delta x). \tag{4}$$

The filter weights are adjusted for the non-uniform vertical spacing using quadratic interpolation in all cases.

The truncated Navier-Stokes with automatic filtering developed by Tantikul & Domaradzki (2010) takes the idea of explicitly-filtered LES further. It achieves grid and filter size independence by only applying the filtering operation when the ratio of kinetic energy contained in the smallest resolved scales to that contained in the large resolved scales exceeds computed theoretical values. The ratio of energy removed $I(\Delta x)/I(2\Delta x)$ by two test-filters with filter widths $\Delta = \Delta x$ denoted by the tilde and $\Delta = 2\Delta x$ denoted by the hat is computed as follows

$$\frac{I(\Delta x)}{I(2\Delta x)} = \int_V \frac{E - \tilde{E}}{E - \widehat{E}} dV \tag{5}$$

$$\approx \int_0^Y \left\langle \frac{\sum_{i=1}^3 \frac{1}{2}(u_i - \tilde{u}_i)(u_i - \tilde{u}_i)}{\sum_{i=1}^3 \frac{1}{2}(u_i - \widehat{u}_i)(u_i - \widehat{u}_i)} \right\rangle (y) dy \tag{6}$$

$$\tilde{u}_i = (Q_5 G_1(\Delta x)) * u_i \tag{7}$$

$$\widehat{u}_i = (Q_5 G_3(2\Delta x)) * u_i \tag{8}$$

$$G_3(2\Delta x) * f \approx \frac{1}{4} f(x-\Delta x) + \frac{1}{2} f(x) + \frac{1}{4} f(x+\Delta x). \tag{9}$$

When this ratio exceeds values obtained for a typical dissipation, inertial, or Batchelor energy spectrum using the same filters – 0.007 to 0.009 from theory as calculated by Tantikul & Domaradzki (2010, 2011) – the filter $Q_5 G_1(\Delta x)$ is applied to the primary variables in physical space to remove this energy imbalance. Using this criterion, the filter is applied automatically at varying intervals centered around 200 time steps for the simulation results presented

Table 1: Resolution and parameters for LES cases and DNS Spalart & Strelets (2000).

	DNS	1% LES
$N_{total} \times 10^6$	14.7	0.18
% of DNS	**100**	**1.25**
Δx^+ at $x = 7$	12	54
Δy^+ at $x = 7$	≤ 1	0.27
Δz^+ at $x = 7$	6.3	34

here, corresponding to approximately 0.5% of one non-dimensional time unit $t = t^* \frac{U_0}{L_x}$.

To serve as a baseline comparison, the dynamic Smagorinsky model is implemented following the description in Sagaut (2006). Simpson's rule is used as the test-filter in the dynamic procedure:

$$\widehat{f}(x) \approx \frac{1}{6} f(x-\Delta x) + \frac{2}{3} f(x) + \frac{1}{6} f(x+\Delta x). \tag{10}$$

Spatial averaging in all directions using a three-point stencil is used in tandem with clipping to avoid rapidly oscillating, or negative values of the dynamic constant.

RESULTS

LES of a laminar separation bubble over a flat plate were performed at 1% of the corresponding DNS benchmark resolution. Two explicitly-filtered LES with approximate deconvolution filters using different weights are performed (F1, F2), along with a truncated Navier-Stokes simulation with automatic filtering (TNS). A simulation with the dynamic Smagorinsky model (DSM) is performed to compare the performance of filtered LES to LES with a SGS model. Simulations are started from the same laminar initial conditions and are run until turbulent flow is well established downstream of reattachment before starting to collect statistics. Results are time-average over 40 non-dimensional time units $t = t^* \frac{U_0}{L_x}$, well beyond the point of reaching averaging-period independence. Parameters for these simulations are summarized in Table 1.

At this coarse resolution, the strong damping provided by the filter in F1 results restricts any generated turbulence to quasi-2D behavior. The obtained laminar separation bubble has a clear shedding frequency and large change in size bearing many similarities to the equivalent 2D problem. This is visible in its pressure and skin friction curves shown in figures 2a and 2b: the expected sharp changes near $x = 4$ are smeared from $x = 3$ to $x = 5$. LES with the DSM underpredicts the peak negative skin friction and reattachment point by 17% and 4.4% respectively as evidenced in figure 2b. It deviates from DNS results downstream of $x = 3$, resulting in a mean velocity profile at 3.5 with a stronger reverse flow near the wall visible in figure 6a. Despite this deviation, it recovers the turbulent skin friction downstream of reattachment very accurately. The TNS and F2 simulations capture the peak negative skin friction with less than 4% error, but over-predict the skin friction immediately after reattachment by approximately 10%. TNS and F2 also recover the mean velocity profile at $x = 3.5$ shown in figure 6 more accurately than the DSM.

The average SGS dissipation contribution $-\tau_{ij}^{\mathrm{SGS}} \bar{S}_{ij}$ of each model and filter is shown in figure 4. Notice that the strongest contributions for all LES are near $x = 3.5$ where the separated shear layer breaks up as is visualized in figure 5 using contours of spanwise vorticity. The effective turbulent eddy viscosity reaches $\nu_{\mathrm{SGS}} \approx 10\nu$ there for the DSM. ν_{SGS} then decreases until it is $O(\nu)$ at reattachment, and further decreases downstream in the turbulent boundary layer. As expected, the models and filters are not active in the laminar and freestream region, but do have some impact inside the separated shear layer as early as $x = 2.5$, corresponding to the earliest non-zero turbulent fluctuations in v' as plotted in figure 3b. The average SGS dissipation provided by the different filters (TNS, F1, F2) is estimated by summing the energy removed each time the automatic filtering operation is triggered as denoted by t_m over one non-dimensional time unit $t = t^* \frac{U_0}{L_x} = N_t \Delta t$ for which the filter is triggered $M \approx N_t/200$ times for TNS, and $M = N_t$ for F1 and F2:

$$-\langle \tau_{ij}^{\mathrm{SGS}} \bar{S}_{ij} \rangle \approx \frac{1}{N_t \Delta t} \sum_{m=1}^{M} \left[E - \tilde{E} \right]_{t=t_m} \tag{11}$$

$$= \frac{1}{N_t \Delta t} \sum_{m=1}^{M} \left[\sum_{i=1}^{3} \frac{1}{2} (u_i - \tilde{u}_i)(u_i - \tilde{u}_i) \right]_{t=t_m} \tag{12}$$

This estimate is not representative of the dynamics of the TNS approach, but it would seem to indicate that its average dissipation contribution is one order of magnitude smaller than the DSM. The maximum effective viscosity of the TNS approach is $O(\nu)$ and is located aft of $x = 3.5$. Its downstream location and negligible contributions before $x = 3$ may explain why TNS results better capture the onset of the peak negative skin friction. The dissipation due to the filter F2 is even smaller, which leads to its slightly later reattachment point seen in the second zero crossing of its C_f curve in figure 2b, and its consistent over-prediction of $\mathrm{v}'_{\mathrm{max}}$ immediately downstream of reattachment in figure 3b. Only the filtered simulations TNS and F2 accurately capture the peak $\mathrm{u}'_{\mathrm{max}}$ and $\mathrm{v}'_{\mathrm{max}}$ in figure 3. The higher viscosity in the DSM damps these fluctuations excessively until the flow reattaches and a turbulent boundary layer develops. The effective numerical viscosity due to the F1 filter is of $O(\nu)$ over a much larger domain spanning $x = 3$ to $x = 5$ explaining previous discrepancies seen in C_f and C_p. Its much larger $\mathrm{u}'_{\mathrm{max}}$ is due to the much stronger 2D shedding causing large periodic changes in the location of transition to turbulence.

CONCLUSIONS

LES of a laminar separation bubble flow over a flat plate were performed at 1% of the benchmark DNS resolution of Spalart & Strelets (2000) using a spectral solver to unambiguously assess the performance of explicitly filtered LES and compare it to the dynamic Smagorinsky model. The truncated Navier-Stokes (TNS) approach recovered the benchmark DNS pressure and skin friction distributions most accurately, followed closely by the sharper explicitly-filtered LES (F2) and the dynamic Smagorinsky model (DSM). The good performance of the TNS and F2 LES provides further support to the concept that filtering

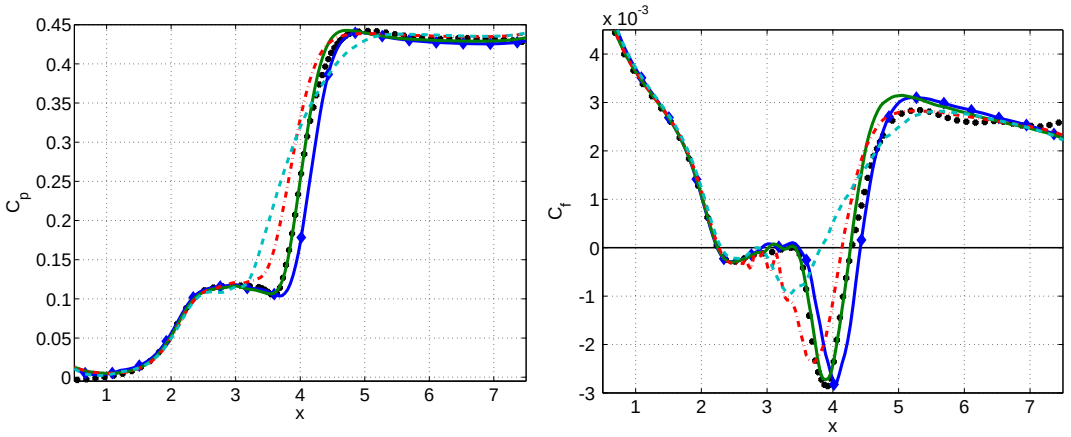

(a) Pressure coefficients.

(b) Skin-friction coefficients.

Figure 2: C_p and C_f. Circles: DNS by Spalart & Strelets (2000); red dash-dotted line: DSM; teal dashed line: F1; blue line with diamonds: F2; green line: TNS.

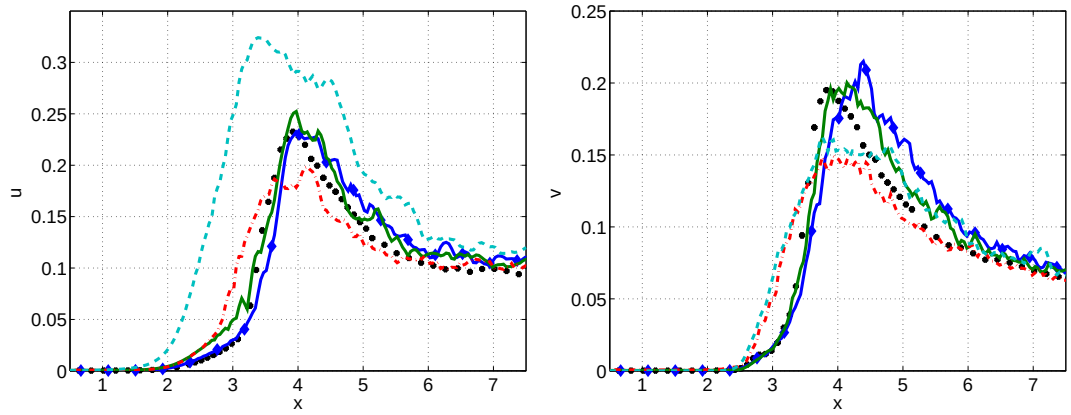

(a) $u'_{max}(x)$.

(b) $v'_{max}(x)$.

Figure 3: Maximum RMS velocity. Circles: DNS by Spalart & Strelets (2000); red dash-dotted line: DSM; teal dashed line: F1; blue line with diamonds: F2; green line: TNS.

can act as an apt replacement for a subgrid-scale model. The poor performance of the F1 explicitly-filtered LES as compared to TNS and F2 is indicative of the dangers associated with the dependence of this approach on the grid and filter size. The automatic filtering criterion framework developed for TNS, wherein filtering is only applied when necessary based on the ratio of energy of the small to the large scales, should help explicit filtering as an SGS model become a more universally applicable and grid-independent methodology. If a solver requires filtering for stability or to remove aliasing error as is common in high-order discretizations, the automatic filtering approach can still be used with a stronger filter to provide further dissipation if and when necessary, such that the combined method becomes grid-independent.

REFERENCES

Alam, M. & Sandham, N.D. 2000 Direct numerical simulation of 'short' laminar separation bubbles with turbulent reattachment. *J. Fluid Mech.* **410**, 1–28.

Bogey, C. & Bailly, C. 2006 Large eddy simulations of transitional round jets: Influence of the Reynolds number on flow development and energy dissipation. *Phys. Fluids* **18** (6), 065101.

Cadieux, F., Domaradzki, J. A., Sayadi, T. & Bose, T. 2014 DNS and LES of laminar separation bubbles at moderate Reynolds numbers. *J. Fluids Eng.* **136** (6).

Canuto, Claudio, Hussaini, M. Y., Quarteroni, Alfio & Zang, Thomas A. 2007 *Spectral Methods : Fundamentals in Single Domains*. Dordrecht: Springer.

Castiglioni, G., Domaradzki, J.A., Pasquariello, V., Hickel, S. & Grilli, M. 2014 Numerical simulations of separated flows at moderate reynolds numbers appropriate for turbine blades and unmanned aero vehicles. *Int. J. Heat Fluid Flow* **49** (0), 91 – 99, 8th Symposium on Turbulence & Shear Flow Phenomena (TSFP8).

Guermond, J.L., Minev, P. & Shen, Jie 2006 An overview of projection methods for incompressible flows. *CMAME* **195** (4447), 6011 – 6045.

Hadžić, I. & Hanjalić, K. 2000 Separation-induced transition to turbulence: Second-moment closure modelling. *Flow Turbul. Combust.* **63** (1-4), 153–173.

Howard, R.J.A., Alam, M. & Sandham, N.D. 2000 Two-

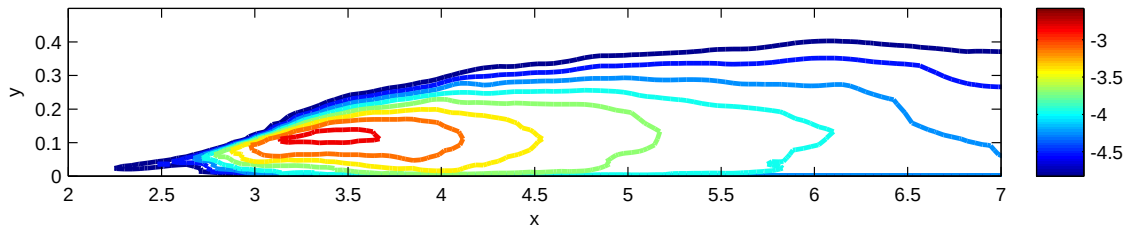

(a) Dynamic Smagorinsky model.

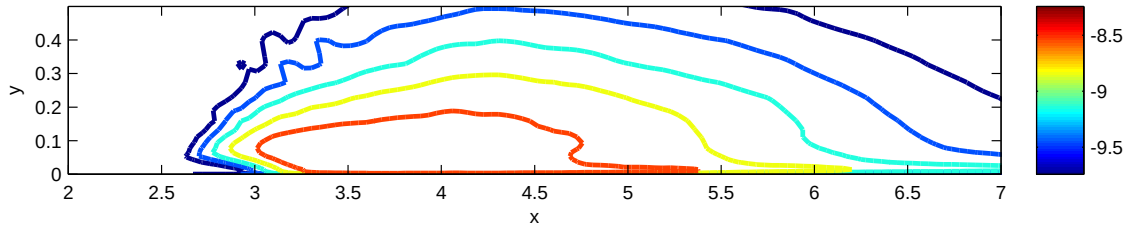

(b) Filter F1.

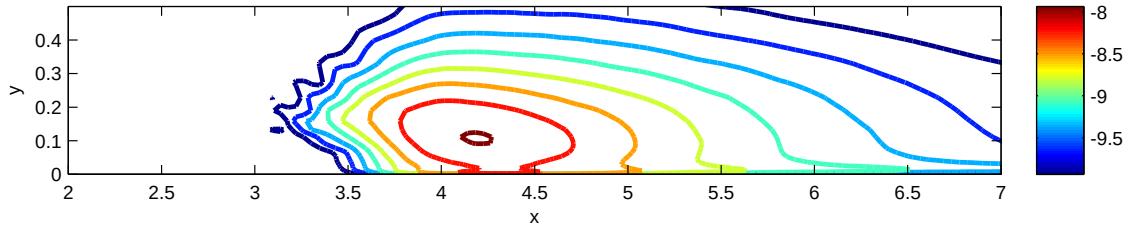

(c) Filter F2.

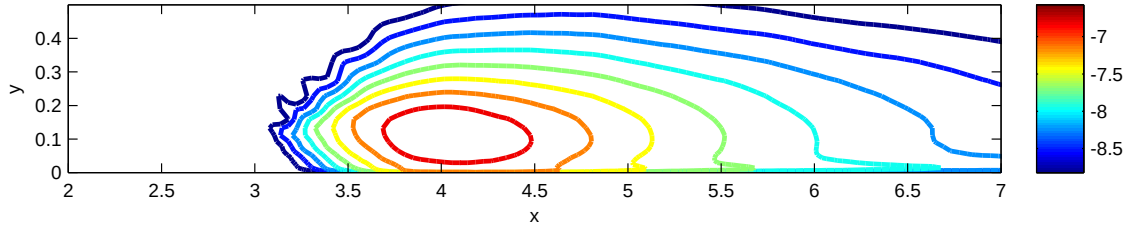

(d) Truncated Navier-Stokes.

Figure 4: Contours of the logarithm of time and spanwise-averaged SGS dissipation $\log_{10}(\langle -\tau_{ij}^{SGS}\bar{S}_{ij}\rangle)$. Each contour represents a jump of 0.25.

equation turbulence modelling of a transitional separation bubble. *Flow Turbul. Combust.* **63** (1-4), 175–191.

Kravchenko, A.G. & Moin, P. 1997 On the effect of numerical errors in large eddy simulations of turbulent flows. *J. Comp. Phys.* **131** (2), 310 – 322.

Minguez, M., Pasquetti, R. & Serre, E. 2008 High-order large-eddy simulation of flow over the ahmed body car model. *Phys. Fluids* **20** (9), –.

Papanicolaou, E. L. & Rodi, W. 1999 Computation of separated-flow transition using a two-layer model of turbulence. *J. Turbomach.* **121** (1), 78–87.

Rizzetta, D. P., Visbal, M. R. & Blaisdell, G. A. 2003 A time-implicit high-order compact differencing and filtering scheme for large-eddy simulation. *Int. J. Numer. Methods Fluids* **42** (6), 665–693.

Sagaut, P. 2006 *Large Eddy Simulation for Incompressible Flows*. Berlin, Germany: Springer.

Spalart, P.R. & Strelets, M.K. 2000 Mechanisms of transition and heat transfer in a separation bubble. *J. Fluid Mech.* **403**, 329–349.

Stolz, S., Adams, N. A. & Kleiser, L. 2001 An approximate deconvolution model for large-eddy simulation with application to incompressible wall-bounded flows. *Phys. Fluids* **13** (4), 997–1015.

Tantikul, T. & Domaradzki, J.A. 2010 Large eddy simulations using truncated Navier-Stokes equations with the automatic filtering criterion. *J. Turb.* **11** (21), 1–24.

Tantikul, T. & Domaradzki, J.A. 2011 Large eddy simulations using truncated Navier-Stokes equations with the automatic filtering criterion: Reynolds stress and energy budgets. *J. Turb.* **12** (34), 1–25.

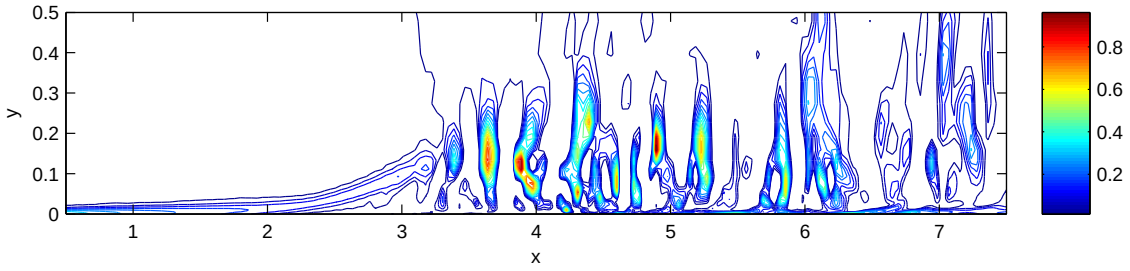

Figure 5: Instantaneous contours of spanwise vorticity for a slice along the x-y plane at $z = 0.3$ from TNS.

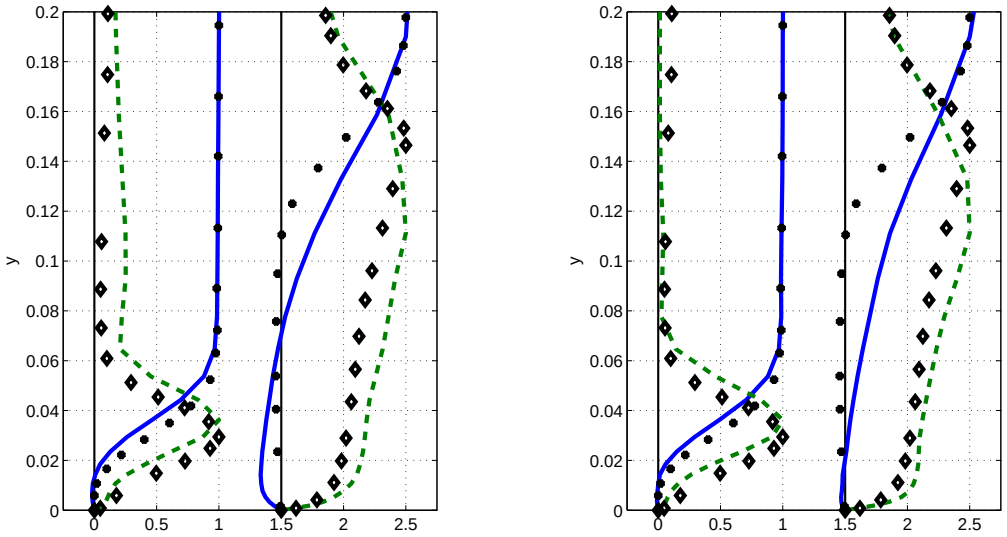

(a) dynamic Smagorinsky.

(b) Filter F1.

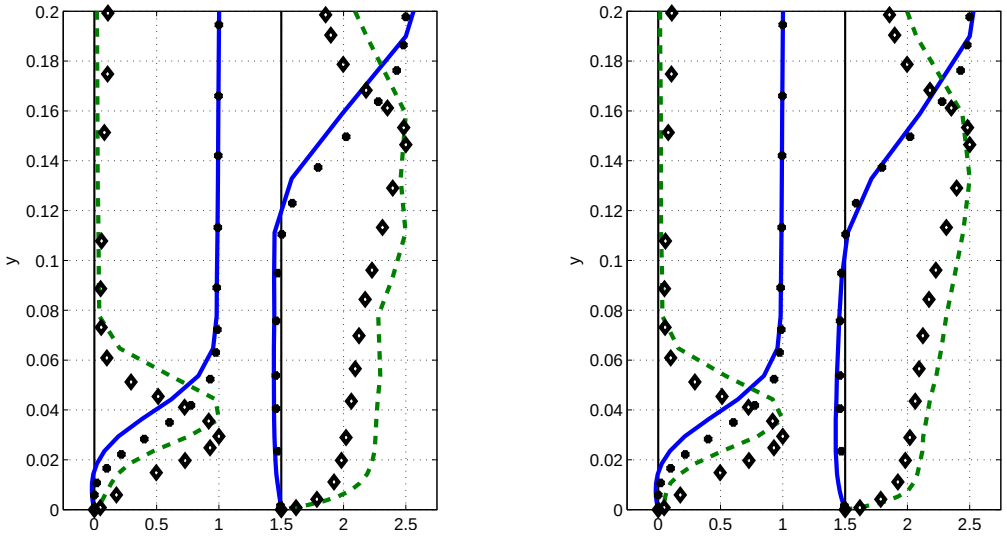

(c) Filter F2.

(d) Truncated Navier-Stokes.

Figure 6: Profiles in LES (lines), and in DNS (symbols). Blue line, black circles: U; green dashed line, black diamonds: $u'/u'_{\max}$. From left to right, plots spaced by 1.5: $x = 2.5$, $x = 3.5$.